

Tuning magneto-dielectric properties of Co_2Z ferrites via Gd doping for high-frequency applications

Jian Wu(武剑), Bing Lu(卢冰), Ying Zhang(张颖), Yixin Chen(陈一鑫), Kai Sun(孙凯), Daming Chen(陈大明), Qiang Li(李强), Yingli Liu(刘颖力), and Jie Li(李颉)

Citation: Chin. Phys. B, 2023, 32 (**9**): 097501. DOI: 10.1088/1674-1056/acc3f7
Journal homepage: http://cpb.iphy.ac.cn; http://iopscience.iop.org/cpb

What follows is a list of articles you may be interested in

Hysteresis loss free soft magnetic ferrites based on Larmor precession

Shuang-Jiu Feng(冯双久), Xin-Li Zhao(赵幸丽), Shou-Jin Zhu(朱守金),Qing-Rong Lv(吕庆荣), Xu-Cai Kan(阚绪材), and Xian-Song Liu(刘先松)

Chin. Phys. B, 2023, 32 (**8**): 087503. DOI: 10.1088/1674-1056/acbdec

Bismuth doping enhanced tunability of strain-controlled magnetic anisotropy in epitaxial $Y_3Fe_5O_{12}$(111) films

Yunpeng Jia(贾云鹏), Zhengguo Liang(梁正国), Haolin Pan(潘昊霖), Qing Wang(王庆), Qiming Lv(吕崎鸣), Yifei Yan(严轶非), Feng Jin(金锋), Dazhi Hou(侯达之), Lingfei Wang(王凌飞), and Wenbin Wu(吴文彬)

Chin. Phys. B, 2023, 32 (**2**): 027501. DOI: 10.1088/1674-1056/ac67cc

Exchange-coupling-induced fourfold magnetic anisotropy in CoFeB/FeRh bilayer grown on $SrTiO_3$(001)

Qingrong Shao(邵倾蓉), Jing Meng(孟婧), Xiaoyan Zhu(朱晓艳), Yali Xie(谢亚丽), Wenjuan Cheng(程文娟), Dongmei Jiang(蒋冬梅), Yang Xu(徐杨), Tian Shang(商恬), and Qingfeng Zhan(詹清峰)

Chin. Phys. B, 2022, 31 (**8**): 087503. DOI: 10.1088/1674-1056/ac673c

Magnetic properties of a mixed spin-3/2 and spin-2 Ising octahedral chain

Xiao-Chen Na(那小晨), Nan Si(司楠), Feng-Ge Zhang(张凤阁), and Wei Jiang(姜伟)

Chin. Phys. B, 2022, 31 (**8**): 087502. DOI: 10.1088/1674-1056/ac5885

Enhancement of magnetic and dielectric properties of low temperature sintered NiCuZn ferrite by Bi_2O_3-CuO additives

Jie Li(李颉), Bing Lu(卢冰), Ying Zhang(张颖), Jian Wu(武剑), Yan Yang(杨燕), Xue-Ning Han(韩雪宁), Dan-Dan Wen(文丹丹), Zheng Liang(梁峥), and Huai-Wu Zhang(张怀武)

Chin. Phys. B, 2022, 31 (**4**): 047502. DOI: 10.1088/1674-1056/ac3399

Tuning magneto–dielectric properties of Co_2Z ferrites via Gd doping for high-frequency applications

Jian Wu(武剑)[1], Bing Lu(卢冰)[1], Ying Zhang(张颖)[1], Yixin Chen(陈一鑫)[1], Kai Sun(孙凯)[1], Daming Chen(陈大明)[2], Qiang Li(李强)[3], Yingli Liu(刘颖力)[1], and Jie Li(李颉)[1,†]

[1] *State Key Laboratory of Electronic Thin Films and Integrated Devices, University of Electronic Science and Technology of China, Chengdu* 610054, *China*
[2] *School of Materials Science and Engineering, Hainan University, Haikou* 570228, *China*
[3] *School of Instrument and Electronics, North University of China, Taiyuan* 030000, *China*

(Received 30 October 2022; revised manuscript received 7 February 2023; accepted manuscript online 14 March 2023)

Magneto–dielectric properties of Co_2Z ferrite materials are tuned via Gd doping for applications in high-frequency antennas and filters in the present work. $Ba_3Co_2Fe_{24-x}Gd_xO_{41}$ ($x = 0.00$, 0.05, 0.10, 0.15, and 0.20) materials are successfully prepared by using solid-state method at 925 °C for 4 h with 2.5-wt% Bi_2O_3 sintering aids. The content of Gd^{3+} ion can affect micromorphology, grain size, bulk density, and magneto–dielectric properties of the ferrite. With Gd^{3+} ion content increasing, saturation magnetization (M_s) first increases and then decreases. The maximum value of M_s is 44.86 emu/g at $x = 0.15$. Additionally, sites occupied by Gd^{3+} ions can change magnetic anisotropy constant of the ferrite. Magnetocrystalline anisotropy constant (K_1) is derived from initial magnetization curve, and found to be related to spin–orbit coupling and intersublattice interactions between metal ions. The real part of magnetic permeability (μ') and real part of dielectric permittivity (ε') are measured in a frequency range of 10 MHz–1 GHz. When $x = 0.15$, material has excellent magneto–dielectric properties ($\mu' \approx 12.2$ and $\varepsilon' \approx 17.61$), low magnetic loss ($\tan\delta_\mu \approx 0.03$ at 500 MHz), and dielectric loss ($\tan\delta_\varepsilon \approx 0.04$ at 500 MHz). The results show that Gd-doped Co_2Z ferrite has broad application prospects in multilayer filters and high-frequency antennas.

Keywords: Co_2Z ferrite, magneto–dielectric properties, Gd doping, high-frequency applications

PACS: 75.50.Gg, 75.47.Lx, 75.60.Ej, 77.22.Ch **DOI:** 10.1088/1674-1056/acc3f7

1. Introduction

With the development of communication systems, miniaturization, integration, multi-function, and high-frequency characteristics of electric equipment are becoming more and more important. These requirements have strengthened the research efforts to develop new electronic materials.[1] Hence, the main goals of the research on electronic materials include achieving high-frequency functionality, high performance, and low-temperature sintering process, especially for the requirements of 5G communication and intelligent electronics. Miniaturized antennas and high-frequency filters are important electronic devices for electronic products and systems.[2–4] The materials that make up the filters need to possess excellent performances, including high magnetic permeability, low magnetic loss, and high-frequency function.[5] For miniaturized antennas, the miniaturization factor ($N = (\mu \cdot \varepsilon)^{1/2}$) is derived from the following relationship:[6] $L_p = c/22f_r\sqrt{\mu\varepsilon}$, where L_p is the length of radiating patch, μ and ε are the magnetic permeability and dielectric permittivity of substrate material, respectively, c is the speed of light in free space, and f_r is the cut-off frequency. Hence, increasing the value of μ, ε, and f_r is the key to reducing the overall size of the antenna. Thus, the utilization of materials with such performances as multilayer filters and antenna substrates should be investigated in more depth.

The $Ba_3Co_2Fe_{24}O_{41}$, often denoted as Co_2Z, is a ferrite material that has a magnetic easy plane perpendicular to the c axis, where the magnetic moments can freely rotate.[7] Hence, this material can possess high magnetization, permeability, permittivity, and cut-off frequency. Singh *et al.* reported the magnetic properties of Co_2Z ferrites doped with SiO_2 and Bi_2O_3 in a frequency range from 1 Hz to 1 MHz.[8] Tran *et al.* doped Co_2Z ferrites with La ions to enhance their microwave absorption and found that La doping endows the ferrites with static magnetic properties and electromagnetic features in a frequency range of 2 GHz–18 GHz.[9] In recent years, many metal ions have been selected for doping Co_2Z ferrite materials to adjust their microstructure and magnetic properties, such as Zn^{2+}, La^{3+}, Mg^{2+}, and Cu^{2+} ions.[10–13] Furthermore, in many studies, ferrite was doped with Ba^{3+} ions, thereby affecting its magnetic properties to a certain extent because Ba^{3+} ions are non-magnetic. The magnetic properties of Co_2Z materials predominantly originate from total magnetic moment of ferrite and superexchange interaction between magnetic ions. Hence, in the present work, we select rare-earth Gd^{3+} ions to replace Fe^{3+} ions and thus adjust magnetic and dielectric properties of resulting ferrites. The magnetism and magnetic properties of obtained ferrites are also discussed in detail.

†Corresponding author. E-mail: lijie@uestc.edu.cn

© 2023 Chinese Physical Society and IOP Publishing Ltd

2. Experimental details

$Ba_3Co_2Fe_{24-x}Gd_xO_{41}$ ferrite materials ($x = 0.00$, 0.05, 0.10, 0.15, and 0.20) were prepared via solid-state reaction by using analytical reagent (AR grade, $\geq 99.5\%$, Aladdin Co.) $BaCO_3$, Co_2O_3, Fe_2O_3, and Gd_2O_3 chemicals as raw materials. These chemicals were combined via ball-milling stoichiometrically. They were mixed with deionized water for 16 h. After being dried at 80 °C and a heating rate of 2 °C/min, these mixtures were pre-sintered at 1200 °C for 4 h. Then, 2.5-wt% Bi_2O_3 was added and mixed with powders using planetary mill for 12 h. The dried powers were granulated using polyvinyl alcohol (PVA) adhesive and then pressed into 2–3-mm-thick plates and columnar samples. Finally, the materials were sintered at 925 °C in air for 4 h.

The phase constitution of the ferrite was identified via x-ray diffraction (XRD, DX-2700, Haoyuan Co.) using Cu-$K\alpha$ radiation. The fractured cross sections of the samples were observed via scanning electron microscopy (SEM, JEOL, JSM-6490). Their bulk densities were measured by using an auto density meter (GF-300D, A & D Co.). Their initial magnetization curve and magnetic hysteresis loops were measured by using a vibrating sample magnetometer (VSM, MODEL, BHL-525) in a direct-current (DC) magnetic field ranging from -10 kOe to $+10$ kOe (1 Oe = 79.5775 A·m^{-1}). Complex magnetic permeability and dielectric permittivity of each sample were measured by using an impedance analyzer (E4991B, Agilent). All the measurements were performed at room temperature.

3. Results and discussion

Figure 1 shows the XRD patterns of materials with different quantities of Gd^{3+} ions. Firstly, as shown by the XRD patterns, all samples exhibit a single hexagonal phase, and no other phases are observed. The crystal structure of Z-type hexagonal ferrite is complex and belongs to $P6_3/mmc$ space group.[14] The XRD patterns in a range of 28°–32° show that the diffraction peaks shift toward a lower angle for the case of Gd doping, indicating that the lattice constant of the doped material is higher than that of the undoped one. The ionic radius of Gd^{3+} is 0.94 Å, which is greater than that of Fe^{3+} ion (0.64 Å). Hence, when a small quantity of Gd^{3+} ions are incorporated, they enter into the crystal lattice and occupy the lattice sites, replacing Fe^{3+} ions. As Gd^{3+} ion content increases to $x = 0.20$, the XRD peaks shift toward higher angles, which illustrates that a large number of incorporated Gd^{3+} ions cause lattice distortion. Hence, the XRD results show that Gd^{3+} ions enter into the lattice cells, and no other phases appear, while Gd doping increases the lattice content and causes lattice to be distorted. Additionally, the materials are prepared at low temperature with 2.5-wt% Bi_2O_3 sintering aids. No Bi_2O_3 phase can be seen in the XRD patterns, which shows that Bi_2O_3 sintering aids provide the energy of chemical reaction, and part of Bi_2O_3 is evaporated.

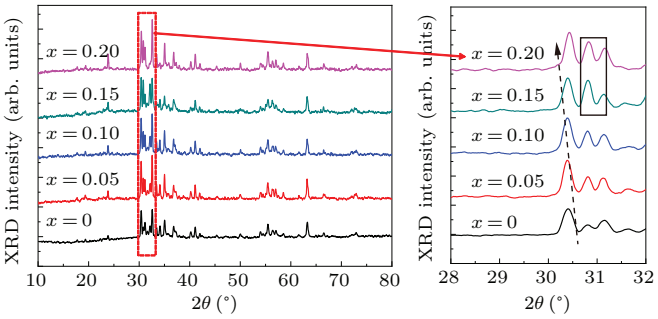


Fig. 1. XRD patterns of materials with different quantities of Gd^{3+} ions.

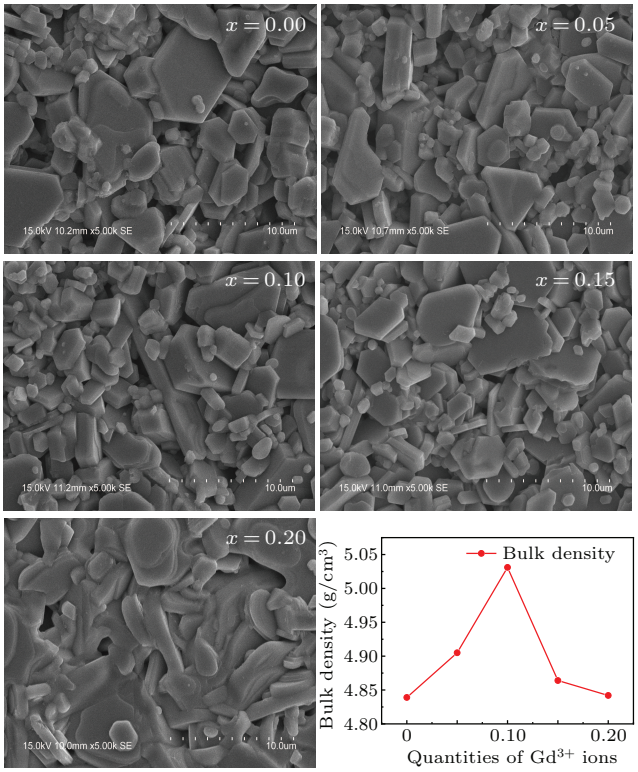


Fig. 2. SEM images and bulk density of materials with different quantities of Gd^{3+} ions.

The SEM images of materials are shown in Fig. 2. These images reveal the presence of hexagonal grains with a platelet-like shape. As Gd^{3+} ion content increases, the grain changes from regular shape into irregular shape. This change is due to the different ionic radii and characteristics of Gd^{3+} and Fe^{3+} ions. The substitution of Gd^{3+} ions for Fe^{3+} ions causes lattice to be distorted, resulting in a change in grain size and shape. The change in grain shape and chemical composition leads to different bulk densities, as shown in Fig. 2. With the quantity of Gd^{3+} ions increasing, the bulk density of the investigated ferrite first increases from 4.83 g/cm^3 ($x = 0.00$) to 5.03 g/cm^3 ($x = 0.10$) and then decreases to 4.84 g/cm^3 ($x = 0.20$). The increase in bulk density is predominantly attributed to two factors: (i) the atomic mass of Gd^{3+} ion is greater than that of

Fe^{3+} ion, and (ii) there are less pores between grain boundaries when $x = 0.10$. When $x = 0.15$ and 0.20, the decrease in bulk density is mainly due to irregular grain shape and the presence of more pores. Additionally, the pores between grain boundaries hinder domain wall from moving, thereby affecting the magnetic properties.

Grain size distributions of materials with different quantities of Gd^{3+} ions are determined from SEM images and the results are shown in Fig. 3. With the quantity of Gd^{3+} ions increasing, the average grain size of materials increases from ~ 2.2 μm ($x = 0.00$) to ~ 3.5 μm ($x = 0.20$). This phenomenon can be attributed to the effect of Gd^{3+} ions on the ferrite. Firstly, Gd^{3+} has greater ionic radius than Fe^{3+}, which leads to larger grains. Secondly, more Gd^{3+} ions exist at the grain boundaries, which makes the shape of grains irregular and larger. In addition, Bi_2O_3 sintering aids can provide the energy required for the chemical synthesis of Co_2Z ferrites. Bi_2O_3 produces a thick liquid phase, which suppresses grain-growing and widens grain boundary, thereby generating a surface tension force in liquid phase and directly affecting grain size and pores.[15]

Figure 4 shows the magnetic hysteresis loops of materials with different quantities of Gd^{3+} ions, and the inset shows a magnified part of the loops in the magnetic field range of $H = 0$ kOe–10 kOe. It can be seen that all samples show relatively smooth hysteresis loops and typical soft magnetic performances. With the quantity of Gd^{3+} ions increasing, saturation magnetization (M_s) of Gd-doped Co_2Z ferrite first increases from 43.66 emu/g ($x = 0.00$) to 44.86 emu/g ($x = 0.15$) and then decreases to 38.57 emu/g ($x = 0.20$). In the basic structure of Co_2Z ferrite, Fe^{3+} ions are distributed on ten different interstitial sublattices, which consist of the following six octahedral (FeO_6) sites: $12k_{VI}$, $4f_{VI}$, $4e_{VI}$, $4f_{VI^*}$, $12k_{VI^*}$, and $2a_{VI}$, three tetrahedral (FeO_4) sites ($4e_{IV}$, $4f_{IV}$, and $4f_{IV^*}$), and one pentahedral (FeO_5) site ($2b_V$) for transition metal ions (including Fe and other metal ions). The main origin of the saturation magnetization is related to the total magnetic moment of the ferrite and the Fe^{3+}–O^2–Fe^{3+} superexchange interaction in the hyper field at 12k and 4f sites.[16] The Gd is a rare-earth element and also a special ferromagnetic element. Its magnetic moment is contributed by the non-filled $4f^7$ electronic shell. The magnetic moment of the Gd^{3+} ion is 7.94 μ_B, which is larger than that of the Fe^{3+} ion (4.9 μ_B). When the Gd^{3+} ions replace the Fe^{3+} ions, the Gd^{3+} ions preferentially occupy the $2a_{VI}$ or $4f_{VI}$ octahedral sites, which results in an increase in the total magnetic moment of the ferrite.[17] Hence, as the Gd^{3+} ion content increases from 0.00 to 0.15, the saturation magnetization increases. Secondly, Wang *et al.* reported that the saturation magnetization is related to the density and average grain size of the ferrite.[18] The result is in good agreement with the above-mentioned trend of density. As a result, the increase in density and average grain size are possibly responsible for the increase in M_s. However, as the quantity of the Gd^{3+} ions increases further, a part of Gd^{3+} ions occupy $4f_{IV^*}$ tetrahedral sites, resulting in a decrease in the total magnetic moment of the ferrite. The change in the bulk density and the presence of pores present two further reasons for the M_s variation. On the other hand, Bi_2O_3 sintering aid is nonmagnetic, so the addition weakened the overall magnetic properties of the Co_2Z ferrite.

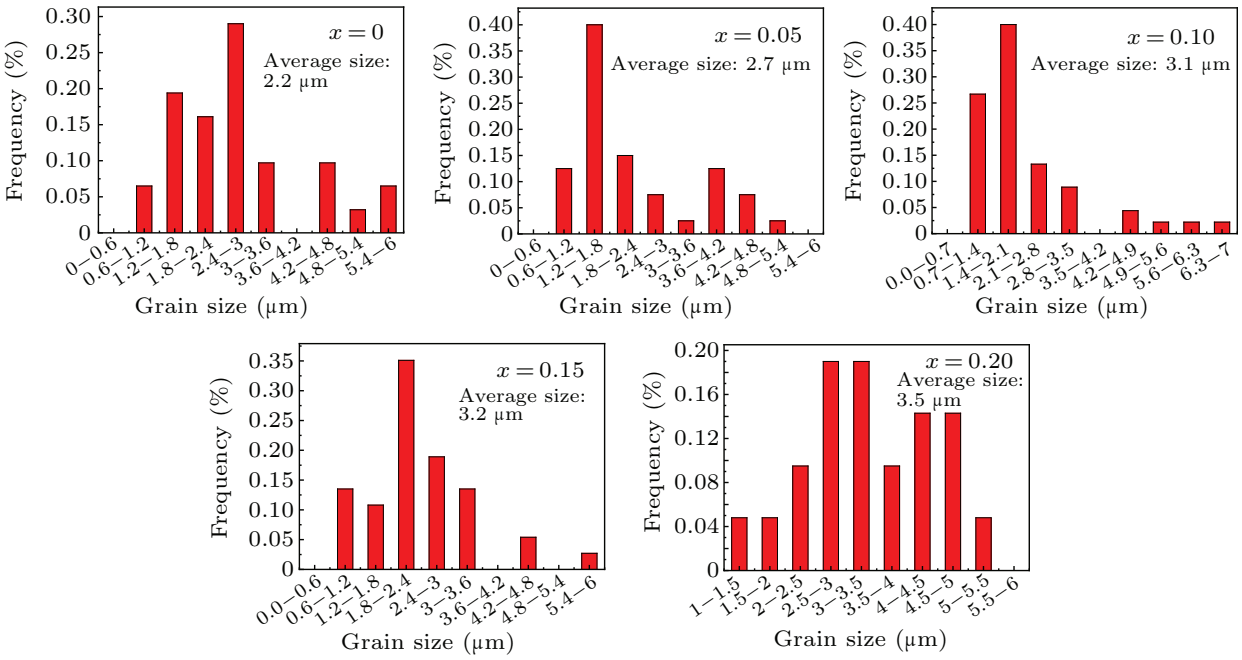


Fig. 3. Grain size distributions of materials with different quantities of Gd^{3+} ions.

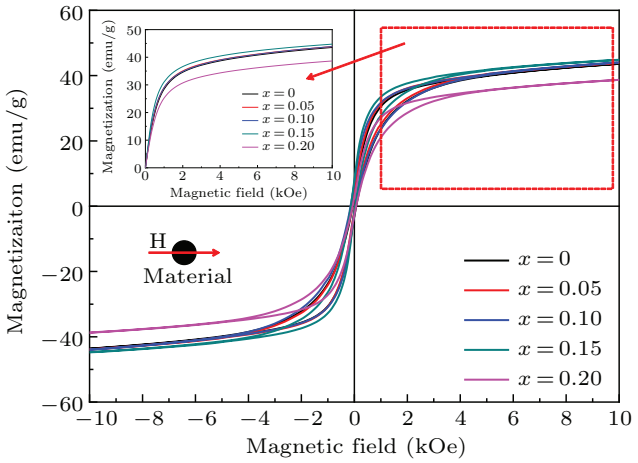


Fig. 4. Magnetic hysteresis loops of materials with different quantities of Gd^{3+} ions.

For ferrite magnetic materials, the initial magnetization of Co_2Z ferrite is related to the magnetocrystalline constant K_1. The initial magnetization curves of materials with different quantities of Gd^{3+} sions are shown in Fig. 5(a). In the initial magnetization curves, the area surrounded by the M–H curve and the M axis (as shown in the inset of Fig. 5(a)) represents the magnetocrystalline anisotropy energy. K_1 can be expressed as the magnetocrystalline anisotropy energy in a unit volume, and obtained from the following equation:

$$K_1 = \frac{1}{V}\int_0^M H\,\mathrm{d}M,$$

where V is the crystal cell volume. The value of K_1 is calculated based on the results in Fig. 5(b). With Gd^{3+} ions doped, the K_1 value is $\sim 6.0 \times 10^4$ J/m^3. Meanwhile, the different values of coercivity (H_c) of samples are obtained from Fig. 5(b). The Gd^{3+} ion doping clearly affects the coercivity of Co_2Z ferrite, and the value of H_c first increases from 55.2 Oe ($x = 0.00$) to 139.7 Oe ($x = 0.10$) and then decreases to 67.4 Oe ($x = 0.20$). It is found that the coercivity of Z-type barium ferrite is mainly affected by anisotropic field and grain size.[19] Among the possible lattice sites that Gd^{3+} ions can occupy, the $2d_v$ fivefold site has the greatest effect on H_c. Therefore, Gd^{3+} ion doping changes the grain size and causes H_c to increase. Incorporated Gd^{3+} ions mainly occupy $2a_{VI}$, $4f_{VI}$, and $4f_{IV^*}$ sites, but these occupancies influence lattice position of $2d_v$ site, leading the lattice to be distorted and affecting the coercivity of material.

For barium ferrite, coercivity is closed related to magnetocrystalline anisotropy. It is found that according to Heisenberg model, the magnetic ion whose orbital is not totally frozen contributes significantly to the magnetocrystalline anisotropy.[20] The magnetic moment of Gd^{3+} ion is larger than that of Fe^{3+} ion. Hence, replacing Fe^{3+} ions with Gd^{3+} ions leads the magnetic properties of the sample to increase slightly but does not cause the number of magnetic ions to increase. Therefore, Gd doping does not cause magnetocrystalline anisotropy constant to change significantly. In addition, it has been reported that the anisotropy of hexaferrite is primarily contributed by Fe^{3+} ions at $2b_V$ sites and Co^{2+} ions.[21] In the above discussion, Gd^{3+} ions mainly occupy $2a_{VI}$, $4f_{VI}$, and $4f_{IV^*}$ sites, which is another reason for the unusual change in magnetocrystalline anisotropy constant. When $x = 0.15$ and 0.20, the decrease in K_1 is due to the presence of small amount of Gd^{3+} ions at grain boundaries and lattice distortion. The contribution of magnetic ions decreases, and the magnetocrystalline anisotropy constant is reduced.

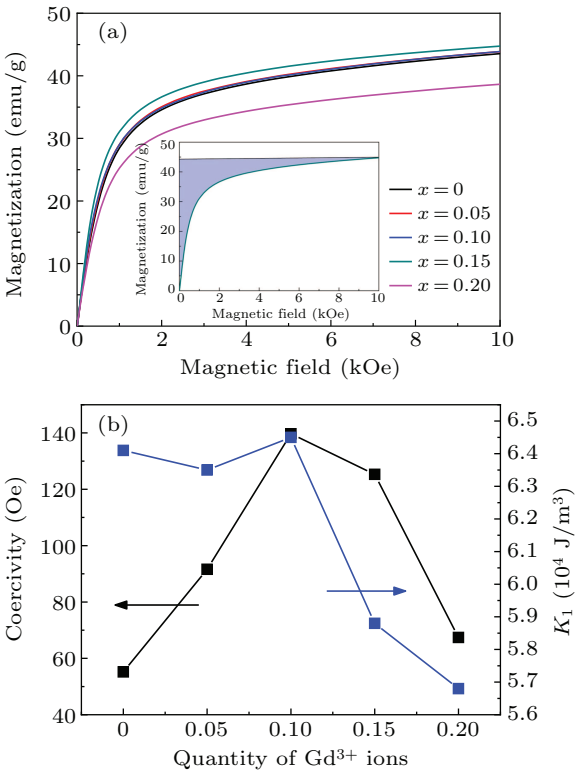


Fig. 5. (a) Initial magnetization curves of materials with different quantities of Gd^{3+} ions, with inset showing integration image and (b) variations of coercivity and K_1 changes with quantities of Gd^{3+} ions.

Figure 6 shows the spectra of the real part of magnetic permeability (μ') and dielectric permittivity (ε') of Gd-doped Co_2Z ferrite in a frequency range from 10 MHz to 1 GHz. For all quantities of Gd^{3+} ions under investigation, the value of μ' first increases and then decreases before the cut-off frequency. The maximum value of μ' (~ 12.2) is found at $x = 0.15$, and this trend is the same as that observed for the saturation magnetization. According to the Globus model, the change in magnetic permeability can be explained according to the following equation:

$$\mu_i \propto \frac{M_s^2 D}{K_1},$$

where D is the average grain size. Therefore, the change in M_s leads the permeability to change. Based on the above discussion, the M_s value is mainly determined by metal ion occupancy, and the K_1 value is dictated by the metal ion properties of $2b_V$ site and 12k site. In addition, the permeability

of ferrite is also affected by grain size. As shown in Fig. 3, the grain size increases gradually with the quantity of Gd^{3+} ions increasing from $x = 0.00$ to $x = 0.15$, which contributes to the enhancement of magnetic permeability. The grain is the largest at $x = 0.20$, but shapes of grains are uneven, and several pores can be observed, which negatively affects magnetic permeability.

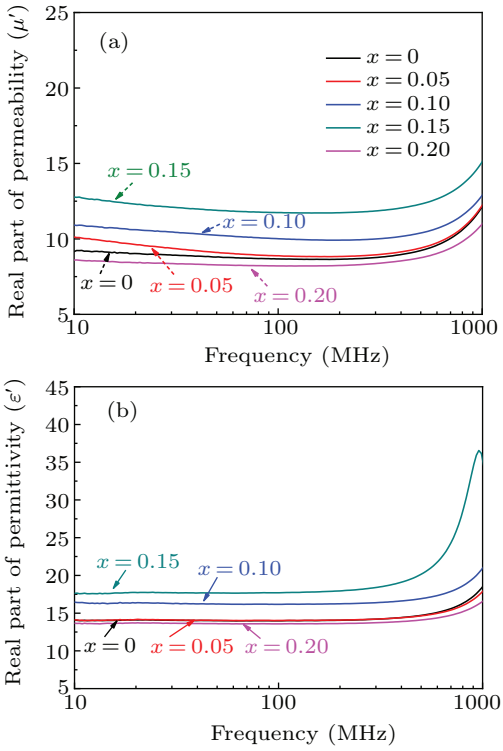


Fig. 6. (a) Real part of magnetic permeability and (b) real part of dielectric permittivity of materials with different quantities of Gd^{3+} ions.

Figure 6(b) shows the variations of real part of dielectric permittivity (ε') with frequency of samples. The values of ε' are almost the same for all samples with a pronounced fluctuation between 13.66 and 17.61 in the frequency range of 10 MHz–1 GHz. The Co_2Z ferrite with $x = 0.15$ has the highest value of ε' (17.61) in all investigated samples. The higher value of ε' can be explained by Koop's model, according to which dielectric structure consists of conduction grains separated by resistive grain boundaries.[22] The surface charge polarization at the interface between grains and grain boundaries is responsible for the higher ε' value. The good dielectric properties of Co_2Z ferrite are due to the hexagonal platelet-like shape particles and the fact that the ion substitution prevents charge from moving. It can be seen that Gd-doped samples exhibit larger grains with more pronounced platelet shape than undoped sample, which provides higher surface area and generates surface polarization. Hence, the value of ε' increases with the quantity of Gd^{3+} ions increasing from 0.00 to 0.15. When $x = 0.20$, grains of different shapes and pores provide more hindrance to domain wall motion and grain conduction, which leads to sharp reduction in dielectric constant.

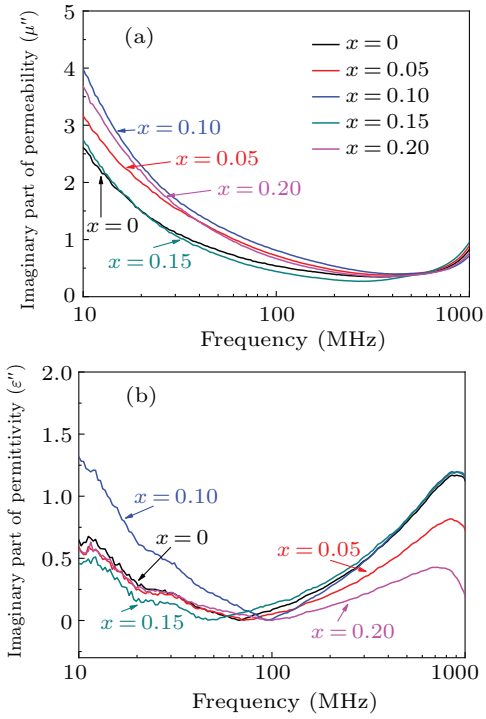


Fig. 7. (a) Variations of imaginary part of magnetic permeability and (b) imaginary part of dielectric permittivity of materials with quantity of Gd^{3+} ions.

Figure 7 shows the variations of imaginary part of magnetic permeability and imaginary part of dielectric permittivity of materials with the quantity of Gd^{3+} ions. As a result, the magnetic loss tangent ($\tan\delta_\mu$) and the dielectric loss tangent ($\tan\delta_\varepsilon$) are obtained from the equation: $\tan\delta_\mu = \mu''/\mu'$ and $\tan\delta_\varepsilon = \varepsilon''/\varepsilon'$. The values of magnetic loss tangent ($\tan\delta_\mu$) and dielectric loss tangent ($\tan\delta_\varepsilon$) of the materials at different frequencies are shown in Table 1. These loss tangents are defined as $\tan\delta_\mu = \mu''/\mu'$ and $\tan\delta_\varepsilon = \varepsilon''/\varepsilon'$, which indicate magnetic and electric energy loss ability, respectively. For ferrite materials, $\tan\delta_\mu$ is contributed by three main components: hysteresis loss tangent $\tan\delta_h$, eddy current loss tangent $\tan\delta_e$, and residual loss tangent $\tan\delta_r$.[23] The $\tan\delta_h$ is the predominant loss at low frequency (in a range of 10 Hz–1 MHz).[10] Hence, the change in magnetic loss at high frequency is attributed to $\tan\delta_e$ and $\tan\delta_r$, while $\tan\delta_e$ is inversely proportional to the DC resistivity, and $\tan\delta_r$ is proportional to the grain size of the ferrite. Smaller grains can provide more grain boundaries and enhance the DC resistivity. The Gd doping increases the grain size (as shown in Fig. 3), which results in an increase of the resistivity, thereby leading the magnetic loss to increase slightly. Additionally, the change of the resistivity not only increases $\tan\delta_e$ but also influences the dielectric loss. The concentration of the Fe^{3+} ions at lattice sites ($2a_{VI}$, $4f_{VI}$, and $4f_{IV^*}$ sites) decreases gradually with the Gd^{3+} content increasing. Therefore, the probability of hopping between Fe^{3+} and Fe^{2+} ions is improved, causing the polarization to increase.[24,25] Furthermore, Bi_2O_3 sintering aids bring the thicker grain boundary, affecting the loss. The uneven shape

of grain and pore affects the magnetic loss and dielectric loss when $x = 0.20$.[26] Besides, the low real permeability and real permittivity are another factors influencing the magnetic and dielectric losses.

Table 1. Values of magnetic loss tangent ($\tan\delta_\mu$), and dielectric loss tangent ($\tan\delta_\varepsilon$) at different frequencies.

Sample	$\tan\delta_\mu$				$\tan\delta_\varepsilon$			
	10 MHz	100 MHz	500 MHz	1 GHz	10 MHz	100 MHz	500 MHz	1 GHz
$x = 0.00$	0.28	0.06	0.04	0.06	0.05	0.06	0.06	0.06
$x = 0.05$	0.31	0.08	0.04	0.07	0.04	0.04	0.04	0.04
$x = 0.10$	0.36	0.08	0.03	0.06	0.05	0.07	0.05	0.05
$x = 0.15$	0.29	0.06	0.03	0.05	0.03	0.07	0.04	0.05
$x = 0.20$	0.31	0.5	0.04	0.08	0.05	0.08	0.06	0.04

4. Conclusions

The Z-type ferrite materials, specifically Gd-doped $Ba_3Co_2Fe_{24-x}Gd_xO_{41}$ with 2.5-wt% Bi_2O_3 sintering aids, are prepared, and their magnetodielectric properties are investigated. Gd doping does not change the phase of Co_2Z ferrite but affects their grain size and shape, contributing to the magnetic and dielectric properties with Gd^{3+} ion substitution. When $x = 0.15$, the $Ba_3Co_2Fe_{22.85}Gd_{0.15}O_{41}$ material processes high saturation magnetization ($M_s = 44.86$ emu/g), low magnetocrystalline anisotropy constant ($K_1 = 5.88 \times 10^3$ J/m^3), high magnetic permeability ($\mu' = 12.2$) and dielectric permittivity ($\varepsilon' = 17.61$), and low magnetic loss and dielectric loss in the frequency range from 10 MHz to 1 GHz. The results indicate that the prepared magnetodielectric materials have great potential applications in high-frequency antennas and filters.

Acknowledgements

Project supported by the National Key Research and Development Program of China (Grant No. 2022YFB3504800), the National Natural Science Foundation of China (Grant Nos. 61901142, 52003256, and 51902037), and the Natural Science Foundation of Shanxi Province, China (Grant No. 201901D211259).

References

[1] Wu H R, Huang F Z, Ti R X, Lu X M, Zhang C Y, Yuan L, Xu Y and Zhang L W 2021 *J. Alloys Compd.* **861** 157996
[2] Hassan Z, Sadiq I, Hussain R, Sadiq F, Idrees M, Hussain S, Riaz S and Naseem S 2022 *J. Alloys Compd.* **906** 164324
[3] Xu J J, Lin P P, Chen Q Q, Zhao X, He P, Lin T S, Jiang C L, Liu Y, Liu H Z and Long W M 2021 *Ceramics International* **47** 973
[4] Lin Y N, Jin L C, Zhang H W, Zhong Z Y, Yang Q H, Rao Y H and Li M M 2020 *J. Magn. Magn. Mater.* **496** 165886
[5] Yang Y, Li J, Zhang H W, Wang G, Rao Y H and Gan G W 2019 *J. Magn. Magn. Mater.* **487** 165318
[6] Gan G W, Zhang D N, Li J, Wang G, Huang X, Yang Y, Rao Y H, Wang X Y and Zhang H W 2020 *Ceramics International* **46** 27996
[7] Huo X Y, Su H, Wang Y, Li Y X and Tang X L 2021 *Ceramics International* **47** 17120
[8] Singh A P, Pandey O P and Sharma P 2022 *Mater. Chem. Phys.* **277** 125574
[9] Tran N, Yang R B, Jeong W H, Manh D H, Phan T L and Lee B W 2022 *J. Am. Ceram. Soc.* **105** 4122
[10] Singh A P, Pandey O P and Sharma P 2021 *Ceramics International* **47** 22550
[11] Manhas A, Kumar A and Singh M 2019 *Proceedings of the National Conference on Recent Advances in Condensed Matter Physics: Racmp-2018* **2093** 020021
[12] Al-Hwaitat E S, Hussein M A, Bsoul I, Buqain R A and Mahmood S H 2019 *Acta Phys. Pol. A* **136** 548
[13] Xu C, Zhang A L, Feng Z J, Lu W L, Kang B J, Zhang J C, Ge J Y and Cao S X 2019 *Phys. Chem. Chem. Phys.* **21** 25826
[14] Zhang X Z, Yue Z X, Meng S Q, Peng B and Yuan L X 2015 *Mater. Res. Bull.* **65** 238
[15] Kalyani B, Pujari N, Edukondalu A, Reddy M S and Vardhani C P 2022 *Chin. J. Phys.* **79** 141
[16] Tran N, Phan T L, Dang N T, Yang D S and Lee B W 2019 *J. Phys. Chem. Solids* **131** 55
[17] Li J, Zhang H W, Li Y X, Li Q and Yu G L 2014 *Journal of Superconductivity and Novel Magnetism* **27** 793
[18] Wang X Y, Zhang H W, Shi L, Li J, Jin L C, Cheng L, Jia L J, Peng R and Zhang D N 2022 *J. Alloys Compd.* **899** 163146
[19] Li J, Hong Y, He S, Li W K, Bai H, Xia Y H, Sun G A and Zhou Z X 2022 *J. Adv. Ceram.* **11** 263
[20] Qi G M, Liu Y L, Chen Y J, Liu Q, Chen J F, Yin Q S and Zhang H W 2021 *J. Mater. Sci.-Mater. El.* **32** 25769
[21] Pullar R C 2012 *Prog. Mater. Sci.* **57** 1191
[22] Singh A P, Pandey O P and Sharma P 2020 *Journal of Superconductivity and Novel Magnetism* **33** 519
[23] Guo Y Q, Wang S Z and Nie Y 2019 *J. Wuhan Univ. Technol.* **34** 1037
[24] Wen D D, Chen X, Luo D S, Lu Y, Chen Y X, Li R P and Cui W 2022 *Chin. Phys. B* **31** 078503
[25] Han J M, Sun L, Cao E S, Hao W T, Zhang Y J and Ju L 2021 *Chin. Phys. B* **30** 096102
[26] Huo X Y, Su H, Zhang Q, Huang F Y, Wu X H, Tang X L, Li Y X and Jing Y L 2023 *J. Alloys Compd.* **933** 167747